The role of the working fluid and non-ideal thermodynamic effects on performance of gas lubricated bearings

de Waart, Wessel; Pini, Matteo

DOI
10.1115/GT2024-127645

Publication date
2024

Document Version
Final published version

Published in
Structures and Dynamics - Aerodynamics Excitation and Damping; Bearing and Seal Dynamics; Emerging Methods in Engineering Design, Analysis, and Additive Manufacturing

Proceedings of ASME Turbo Expo 2024
Turbomachinery Technical Conference and Exposition
GT2024
June 24–28, 2024, London, United Kingdom

GT2024-127645

THE ROLE OF THE WORKING FLUID AND NON-IDEAL THERMODYNAMIC EFFECTS ON PERFORMANCE OF GAS LUBRICATED BEARINGS

Wessel de Waart[1], Matteo Pini[1,*]

[1]Propulsion and Power, Faculty of Aerospace Engineering, Delft University of Technology, The Netherlands

ABSTRACT

Small-scale turbomachinery operating at high rotational speed is a key technology for increasing the power density of energy and propulsion systems. A notable example is the turbine of an organic Rankine cycle turbogenerator for thermal recuperation from prime engines and industrial processes. Such systems typically operate with organic compounds characterized by complex molecular structures, to allow the design of efficient fluid machinery and flexibility in matching the heat source and sink temperature profiles. Gas lubricated bearings are considered advantageous compared to traditional oil-lubricated rolling element bearings for supporting the turbine rotor, enabling greater machine compactness and reduced complexity, and to avoid contamination of the working fluid. In certain operating conditions, however, the lubricant of the gas bearing is in thermodynamic states near the saturated vapor line or in the vicinity of the fluid critical point whereby non-ideal effects are relevant and may affect bearing performance. This work investigates the physics of thin film flows in gas bearings operating with fluids made by complex molecules. The influence of non-ideal thermodynamic effects on gas bearing performance is discussed by analysis of the fluid bulk modulus. Reduced values of the non-dimensional bulk modulus near the critical point or saturated vapor line decrease bearing performance. The main parameter characterizing the influence of molecular complexity on bearing performance is shown to be the acentric factor. For complex fluids with large acentric factors, the impact of non-ideal thermodynamic effects on non-dimensional bearing load capacity and rotor-dynamic characteristics is less pronounced.

Keywords: Gas Bearings, Non-Ideal Thermodynamic Effects, High-Speed Turbomachinery

NOMENCLATURE

Roman letters

c	Non-dimensional damping coefficient [-]
c_0	Nominal bearing clearance [m]
$G_{x,z}$	Turbulence correction factors [-]
h	Film thickness [m]
k	Non-dimensional stiffness coefficient [-]
L	Bearing width [m]
m	Rotor mass [kg]
p	Pressure [Pa]
R	Bearing radius [m]
S	Structural compliance ratio [-]
T	Temperature [K]
w_d	Bump foil deflection [m]
W	Load capacity [N]
x	Circumferential spatial coordinate [m]
X	Coordinate in the inertial frame [m]
Y	Coordinate in the inertial frame [m]
z	Axial spatial coordinate [m]
Z	Thermodynamic compressibility factor [-]

Greek letters

β	Bulk modulus [Pa]
γ	Specific heat ratio [-]
γ_{ex}	Ratio of excitation frequency to rotor speed [-]
γ_{Pv}	Generalized isentropic pressure-volume exponent [-]
γ_S	Structural loss factor [-]
ϵ	Eccentricity ratio [-]
Λ	Bearing compressibility number [-]
μ	Dynamic viscosity [kg m^{-1} s^{-1}]
ρ	Fluid density [kg m^{-3}]
ψ	Attitude angle [rad]
Ω	Rotor speed [rad/s]

Dimensionless groups

Re	Reynolds number

Superscripts and subscripts

0	Steady-state value
1X	Perturbed quantity due to shaft motion in X-direction
1Y	Perturbed quantity due to shaft motion in Y-direction
r	Reduced thermodynamic property
ref	Reference value
$(\bar{\cdot})$	Non-dimensional parameter

*Corresponding author: M.Pini@TUDelft.nl

1. INTRODUCTION

Small-scale turbomachinery operating at high rotational speeds are an enabling technology for the high-power density propulsion and power systems of the future [1]. Machines with tip diameters on the order of $30mm$ and rotor speeds up to $200krpm$ have been considered for a variety of applications [2]. Examples of such applications include small turbochargers [3], cryogenic coolers using an inverse Brayton cycle [4], fuel cell air management systems [5] and micro gas turbines. More recently, high-speed centrifugal compressors have been investigated for both domestic [6] and airborne [7] heat pump applications, whereas radial-inflow turbines are considered for high power-density thermal energy conversion systems based on the super-critical CO_2 Brayton cycle [8] or the organic Rankine cycle (ORC) [1].

The requirements of compactness and high efficiency dictate the adoption of gas bearings in high-speed turbomachinery. This type of bearings can support high-speed rotors with low-maintenance and at reduced friction loss [9]. Furthermore, the use of the process fluid as a lubricant in the gas bearing allows the elimination of the oil lubrication system, thereby avoiding the contamination of the working fluid and reducing the overall system weight and complexity. Gas bearings rely on the relative motion between the rotating shaft and the static bearing components to generate a lubricating film. The amount of load that the bearing can carry therefore depends on fluid properties such as the pressure and viscosity. When applied in turbomachines operating with dense vapors or supercritical flows, compressibility and non-ideal thermodynamic effects can largely affect the bearings performance.

A dense vapor is a fluid in thermodynamic states near the saturated vapor line or near the critical point whereby the compressibility number $Z < 1$ [10]. Such states are characterized by non-ideal thermodynamic effects in which molecular interactions are non negligible. Giuffré et al. [11] recently demonstrated the design optimization of a twin-stage high-speed compressor for an electrically driven vapor compression cycle. The effects of working fluid and non-ideal thermodynamic effects were taken into account in the design procedure by the isentropic pressure-volume exponent. Furthermore, Giuffré and Pini [12] presented design guidelines for axial turbines operating with non-ideal compressible flows. Molecularly complex fluids with low speed of sound lead to supersonic flows in the nozzles of such turbines, which strongly affects fluid dynamic losses. Tosto et al. [13] took a fundamental approach to study how loss mechanisms in internal flows are influenced by both the fluid molecular complexity and the non-ideal thermodynamic effects.

Most of the available scientific literature on gas foil bearings considers cases in which air at sea-level conditions is utilized as lubricant. NASA performed an extensive experimental campaign [9] to show the feasibility of supporting high-speed rotors using gas foil bearings lubricated with air. Measured data was used to derive approximate relations for bearing load capacity [14] as well as linearized rotordynamic coefficients [15]. Heshmat et al. [16] presented a modeling technique for bump type gas foil journal bearings in which the compliant bump strip layer was modeled as an elastic structure. Recent works investigated the performance of hydrodynamic bearings lubricated with dense vapors. Bruckner [17] experimentally investigated the windage losses in gas foil bearings operating at high-pressure. Losses associated to inertia effects were shown to increase significantly at elevated pressures. Conboy [18] numerically investigated the performance of gas foil thrust bearings applied in a S-CO_2 closed-Brayton cycle laboratory setup of Sandia National Laboratories. The developed numerical model was coupled to a thermodynamic software program [19] to compute the thermo-physical fluid properties. Kim [20] presented a high-level 3D thermohydrodynamic model of a radial foil bearing including turbulence and non-ideal thermodynamic effects. In spite of the increasing body of literature, there have been only a few fundamental studies aimed at elucidating the significance of non-ideal thermodynamic effects and molecular complexity on the physical behavior of thin film flows in gas bearings.

Guenat and Schiffmann [21] investigated the impact of non-ideal thermodynamic effects on gas bearing performance. In their work, a numerical study was performed indicating how the non-dimensional load capacity and bearing stability are affected by the thermodynamic state of the fluid. The non-dimensional bulk modulus was identified as the main thermo-physical parameter affecting the density distribution in the gas film. Results were presented for gas bearings lubricated with various refrigerant fluids. However, the relation between the non-dimensional bulk modulus and the non-ideal thermodynamic effects was not explicitly addressed. Furthermore, the influence of the fluid molecular structure on bearing performance is not yet fully understood. These aspects are investigated in this work. A physical interpretation of the non-dimensional bulk modulus in the context of flows in a non-ideal thermodynamic state is presented. Furthermore, the influence of molecular complexity on the non-dimensional bearing load capacity and rotor-dynamic characteristics is elucidated using an analysis based on scaling principles and a cubic equation of state.

The article is structured as follows. Section 2 presents the compressible Reynolds equation which is solved numerically using a finite difference method. The perturbation method used to obtain the linearized rotor-dynamic stiffness and damping coefficients is also presented. The outlined methods are used to calculate results for both rigid bearings and gas foil bearings. In section 3, the influence of non-ideal thermodynamic effects and molecular complexity on bearing performance is discussed. Finally, the main conclusions drawn from this study are outlined in section 4.

2. METHODOLOGY

Both rigid journal bearings and gas foil journal bearings are modeled. The compressible Reynolds equation governing the density distribution within the thin film is presented. A simple elastic model is utilized to account for the bump foil deflections in gas foil bearings. The non-dimensional load capacity and critical mass are introduced as the bearing performance parameters used to analyze the influence of non-ideal thermodynamic effects and molecular complexity.

2.1 Flow Modeling

The thin film flow separating the rotating shaft from the top foil is modeled using the Reynolds equation. The Reynolds equation was first derived in 1886 by Osborne Reynolds for incompressible flow from the equations of conservation of mass and momentum [22]. Chien et al. [23] present a derivation of the steady Reynolds equation for two-dimensional compressible flows of high-pressure gasses. The derivation can be extended to include unsteady effects and three-dimensional flows, leading to the compressible Reynolds Equation (1) as used in this work:

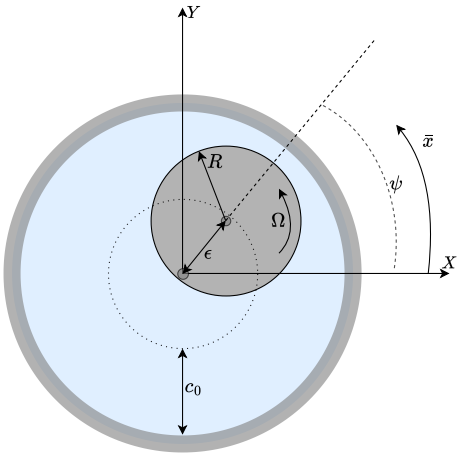

FIGURE 1: SCHEMATIC FIGURE SHOWING A RIGID JOURNAL BEARING.

$$\frac{\partial}{\partial \bar{x}}\left(\frac{\bar{\beta}\bar{h}^3}{\bar{\mu}}G_x\frac{\partial \bar{\rho}}{\partial \bar{x}}\right)+\frac{\partial}{\partial \bar{z}}\left(\frac{\bar{\beta}\bar{h}^3}{\bar{\mu}}G_z\frac{\partial \bar{\rho}}{\partial \bar{z}}\right)=\Lambda\frac{\partial(\bar{\rho}\bar{h})}{\partial \bar{x}}+2\Lambda\frac{\partial \bar{\rho}\bar{h}}{\partial \bar{t}}. \quad (1)$$

Some of the nomenclature related to the bearing geometry is shown in Figure 1. The spatial coordinates in the circumferential and axial directions are normalized by the shaft radius, whereas the film thickness is normalized using the nominal bearing clearance. The non-dimensional bearing compressibility number or bearing speed number is written as:

$$\Lambda=\frac{6\mu_{ref}\Omega R^2}{p_{ref}c_0^2}. \quad (2)$$

The bearing compressibility number is defined in terms of the rotor speed, the thermodynamic state of the fluid in the bearing compartment, and the bearing geometry. The Poiseuille-like terms on the left-hand side of Equation (1) represent the effect of pressure gradients on the flow in the circumferential and axial directions. These diffusive effects tend to attenuate the density gradients and are more pronounced for low compressibility numbers Λ. For increasing compressibility numbers, the first right-hand side term of Equation (1), becomes relevant. This Couette-like term denotes the effect of viscous stresses dragging the fluid into an aerodynamic wedge, thereby causing regions of increased density (and pressure) near the location of minimum film thickness. In this work, the compressibility number will be used as an independent parameter for analyzing bearing performance.

Traditionally, most literature on gas bearings deals with air-lubricated bearings at low pressure, characterized by laminar thin films and thermodynamic state properties calculated with the ideal gas law. In high-pressure lubrication flows, however, the local Reynolds number can reach levels where instabilities arise in the laminar thin film leading to flow transition and turbulence. Although the physics of transition and turbulence is not well represented by a Reynolds-type equation, it has become common practice to account for turbulence effects by means of empirical correction factors. These turbulence correction factors (G_x and G_z) arise in the Poiseuille flow terms of the Reynolds Equation (1). Several theoretical approaches have been proposed to derive expressions for the semi-empirical correction factors [24] [25] [26]. In the model of Constantinescu, the semi-empirical correction factors G_x and G_z are written as:

$$\begin{aligned} G_x &= \left(1+\frac{\alpha_x}{12}Re^{\beta_x}\right) \\ G_z &= \left(1+\frac{\alpha_z}{12}Re^{\beta_z}\right), \end{aligned} \quad (3)$$

with the empirical constants $\alpha_x = 0.0136$, $\beta_x = 0.90$, $\alpha_z = 0.0043$ and $\beta_z = 0.96$. It should be noted, however, that the different theories mentioned here all lead to the same qualitative behavior of the turbulence correction factors as a function of the local Reynolds number.

2.2 Thermo-physical Property Models

The compressible Reynolds Equation (1) constitutes a second-order non-linear partial differential equation for the non-dimensional density field defined as $\bar{\rho} = \rho/\rho_{ref}$. The subscript ref refers to some representative thermodynamic reference state, typically corresponding to the state of the fluid surrounding the bearing. Apart from the density, the thermo-physical properties appearing in the Reynolds equation are the normalized dynamic viscosity $\bar{\mu} = \mu/\mu_{ref}$ and the non-dimensional bulk modulus $\bar{\beta} = \beta/p_{ref}$. The bulk modulus of the fluid is defined as the inverse of the isothermal compressibility and is given as:

$$\beta=\rho\left.\frac{\partial p}{\partial \rho}\right|_T. \quad (4)$$

The fluid dynamic performance of turbomachinery components operating with working fluids in non-ideal thermodynamic states is often characterized [10] in terms of the specific heat ratio γ and the generalized pressure-volume exponent γ_{Pv}. The latter is used in place of γ to describe isentropic flows in which non-ideal thermodynamic effects are of interest such that:

$$\left(\frac{p}{\rho}\right)^{\gamma_{Pv}}=\text{const.} \quad (5)$$

Differentiation of the above relation yields [13] the following relation between the isothermal compressibility or non-dimensional bulk modulus of the fluid and the parameters γ and γ_{Pv}:

$$\gamma_{Pv}=\frac{\rho}{p}\left.\frac{\partial p}{\partial \rho}\right|_s=\gamma\frac{\rho}{p}\left.\frac{\partial p}{\partial \rho}\right|_T=\frac{\beta\gamma}{p}=\bar{\beta}\gamma. \quad (6)$$

The value of the non-dimensional bulk modulus is therefore related to the level of non-ideality of the fluid state. In thermodynamics, the fluid compressibility factor Z is often used as a measure of non-ideality of a gas. The compressibility factor is defined such that:

$$p = Z\rho RT. \tag{7}$$

From the definitions of Z the following relation can be derived between the non-dimensional bulk modulus and the compressibility factor:

$$\bar{\beta} = 1 + \frac{\rho_r}{Z}\frac{\partial Z}{\partial \rho_r}\bigg|_T. \tag{8}$$

From Equation (8), both the non-dimensional bulk modulus and the compressibility factor are one for ideal gasses. The qualitative behavior of both parameters can be explained based on the inter-molecular potential. As the pressure of a gas is increased the distance between molecules decreases and the inter-molecular forces become more significant. In particular, attractive forces between molecules start to dominate. This causes both Z and $\bar{\beta}$ to drop below one. At large pressures, the volume of the molecules becomes non-negligible with respect to the molar volume of the fluid. At low molar volumes, this causes the repulsive forces between molecules to become more significant. When the attractive and repulsive forces are balanced, the compressibility factor Z reaches a minimum and the non-dimensional bulk modulus rises above $\bar{\beta} = 1$. Upon further increase of the density, both the bulk modulus and compressibility factor increase. Contours of the non-dimensional bulk modulus are plotted on the reduced *T-s* thermodynamic plane in Figure 2 for siloxane MM. The plot shows a strong reduction of the non-dimensional bulk modulus in the vicinity of the critical point. In the limit of the critical point, the bulk modulus reaches a value of zero. For very high pressures in the supercritical domain, values larger than one are attained. In this region, sometimes considered the 'liquid-like' part of the supercritical domain, the fluid behaves increasingly like an incompressible medium. For an ideal gas, the bulk modulus reduces to the pressure and $\bar{\beta}$ is equal to one:

$$\bar{\beta}_{ref} \equiv \frac{\rho_{ref}}{p_{ref}}\frac{\partial p}{\partial \rho}\bigg|_T = \frac{\rho_{ref}}{p_{ref}} RT_{ref} = 1 \quad \text{for an ideal gas.} \tag{9}$$

The non-dimensional bulk modulus and dynamic viscosity both depend on the thermodynamic state of the fluid. Traditionally, the thin film flows in gas (foil) bearings have been modeled under the assumption of isothermal flow. The bulk modulus and viscosity are therefore evaluated as a function of the local density and the reference temperature, i.e. $\bar{\beta}\left(\rho, T_{ref}\right)$ and $\bar{\mu}\left(\rho, T_{ref}\right)$. The non-linear Reynolds equation is solved iteratively, and the thermo-physical properties are updated after each iteration using the density distribution in the film.

For ideal gas lubrication, the dynamic viscosity is typically evaluated using Sutherland's law and only depends on the temperature. Furthermore, for isothermal flow, the non-dimensional bulk modulus reduces to the non-dimensional density. This allows for a straightforward solution of the Reynolds equation without the necessity of coupling the solver to an external software program for the calculation of thermo-physical fluid properties.

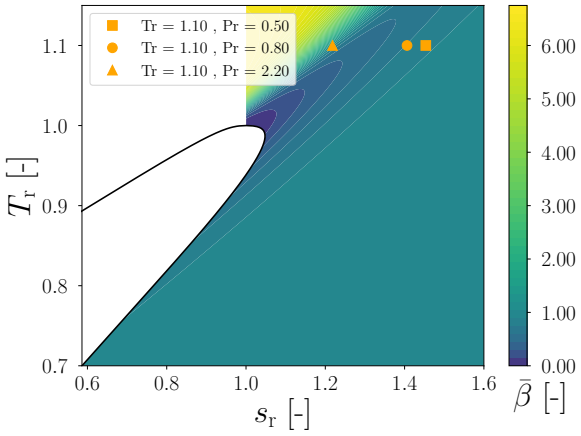

FIGURE 2: CONSIDERED OPERATING CONDITIONS SHOWN ON THE REDUCED T-S THERMODYNAMIC PLANE OF SILOXANE MM ALONG WITH CONTOURS OF THE NON-DIMENSIONAL BULK MODULUS $\bar{\beta}$. PLOT GENERATED USING NICEPROP [27].

In this work, the thermodynamic properties of dense vapors and supercritical fluids are computed using equation of state models of varying complexity. The Peng-Robinson cubic equation of state is used to derive theoretical insight. The limited number of parameters involved in the cubic equation of state allows for identifying the most relevant fluid properties relating the molecular complexity to the bearing performance. More complex Helmholtz free energy based multi-parameter equations of state are used to confirm the results. Correlations are used to model the variation of the dynamic viscosity with temperature and density. The implementation of both the equations of state and the correlations for the dynamic viscosity is done using the CoolProp [28] and RefProp [19] software programs.

2.3 Foil Modeling

For gas foil bearings, the increased pressures in the gas film lead to a net force on the top and bump foil structure. The bump foil is a compliant structure that will deform elastically under the action of such forces, resulting in a change in the local film thickness. The foil deflections are accounted for using a simple elastic model. In the model, a linear relation is used between the bump foil deflections w_d and the pressure. The method is well established in literature (e.g. [16] and [29]) and is not repeated here. It is noted that more accurate models for the bump and top foil deflections exist in literature (e.g. [30]). The aim of the current work, however, is to investigate the fundamental non-ideal thermodynamic effects in the fluid film. For simplicity, the analysis is carried out using this linear elastic model.

Accounting for the structural deflections, the steady-state non-dimensional film thickness can be written as:

$$\bar{h}_0 = 1 - \epsilon\cos\left(\bar{x} - \psi\right) + S\delta\bar{p}_0, \tag{10}$$

where the structural compliance factor [29] is defined as:

$$S = \frac{P_{ref}}{c_0 K_f}. \tag{11}$$

2.4 Perturbation Method

The unsteady Reynolds Equation (1) allows for predicting the time-varying reaction forces exerted by the fluid film on the rotor shaft. The equation can be coupled to the non-linear rotor-dynamic equations of motion in order to model the evolution of the rotor orbits in time. In this work, however, only the potential onset of bearing instabilities is considered and not the evolution of the unstable rotor motions. Therefore, a perturbation method is applied where a small harmonic motion is introduced around the equilibrium rotor position. The perturbation in the rotor position will introduce a perturbation in the pressure field and the structural deflections of the bump foils, which can eventually lead to instabilities. The perturbed film thickness including the harmonic motions and perturbed foil deflections is written as:

$$\bar{h} = \bar{h}_0 - \epsilon_{1X} cos\,(\bar{x})\, e^{i\gamma_{ex}\bar{t}} - \epsilon_{1Y} sin\,(\bar{x})\, e^{i\gamma_{ex}\bar{t}} + \frac{S}{(1+i\gamma_S)} \left(\delta\bar{p}_{1X}\epsilon_{1X} + \delta\bar{p}_{1Y}\epsilon_{1Y}\right) e^{i\gamma_{ex}\bar{t}} \tag{12}$$

The subscript 0 indicates parameter values at the rotor steady-state equilibrium position, whereas the subscript 1 indicates the perturbations from the steady-state. The rotor motion in X- and Y-directions refers to the inertial axes as shown in Figure 1. The parameter γ_{ex} is defined as the excitation frequency normalized using the shaft rotational speed Ω. The perturbation in the film thickness will result in a perturbation in the density field as well as the ratio of the bulk modulus to dynamic viscosity appearing in the Reynolds equation:

$$\bar{\rho} = \bar{\rho}_0 + \epsilon_{1X}\bar{\rho}_{1X} e^{i\gamma_{ex}\bar{t}} + \epsilon_{1Y}\bar{\rho}_{1Y} e^{i\gamma_{ex}\bar{t}} \tag{13}$$

$$\frac{\bar{\beta}}{\bar{\mu}} = \bar{\kappa}_{Te} = \bar{\kappa}_{Te0} + \epsilon_{1X}\left(\frac{\partial\bar{\kappa}_{Te}}{\partial\bar{\rho}}\right)_0 \bar{\rho}_{1X} e^{i\gamma_{ex}\bar{t}} + \epsilon_{1Y}\left(\frac{\partial\bar{\kappa}_{Te}}{\partial\bar{\rho}}\right)_0 \bar{\rho}_{1Y} e^{i\gamma_{ex}\bar{t}}, \tag{14}$$

where the effective bulk modulus $\bar{\kappa}_{Te}$ is defined following the work of Chien et al. [23] as the ratio of the bulk modulus to dynamic viscosity. It is used here only as a short-hand notation. The partial derivative of the effective bulk modulus to density at constant temperature is written using the chain rule:

$$\left.\frac{\partial\kappa_{Te}}{\partial\rho}\right|_T = \frac{\kappa_{Te}}{\rho} + \frac{\rho}{\mu}\left.\frac{\partial^2 p}{\partial\rho^2}\right|_T - \frac{\kappa_{Te}}{\mu}\left.\frac{\partial\mu}{\partial\rho}\right|_T. \tag{15}$$

Finally, the turbulence correction factors are a function of the local Reynolds number and therefore of the density, film thickness, and viscosity. The perturbed turbulence correction factors can be obtained in a similar way by application of the chain rule.

The perturbed quantities can be substituted into the unsteady Reynolds Equation (1). The zeroth- and first-order terms can be grouped and separated leading to the zeroth-order or steady-state Reynolds equation (for $\bar{\rho}_0$) and two first-order or perturbed Reynolds equations (for $\bar{\rho}_{1X}$ and $\bar{\rho}_{1Y}$). The equations are presented in Appendix A. The equations are discretized using a finite difference method. The non-linear steady-state equation is solved iteratively. The thermodynamic properties and bump foil deflections are updated after every iteration. The first-order equations can be solved straightforwardly, once the steady-state solution is obtained. For both the steady-state and the perturbed Reynolds equations a periodic boundary condition is applied in the circumferential direction. Dirichlet boundary conditions are applied in the axial direction, imposing the ambient (steady-state) density with zero perturbation at the sides of the bearing.

2.5 Bearing Performance Parameters

Once the steady-state and perturbed density fields are obtained, the pressure field is computed as a function of the density field and the reference temperature. The components of the non-dimensional load capacity are computed as:

$$W_\alpha = -\int_{-L/D}^{L/D}\int_0^{2\pi} \bar{p} H_\alpha d\bar{x} d\bar{z}, \tag{16}$$

$$W = \sqrt{W_x^2 + W_y^2}. \tag{17}$$

The non-dimensional dynamic bearing impedances can be obtained by integration of the non-dimensional perturbed pressure field in a similar way:

$$k_{\alpha\beta} + \gamma_{ex} c_{\alpha\beta} = -\int_{-L/D}^{L/D}\int_0^{2\pi} \bar{p}_{1\beta} H_\alpha d\bar{x} d\bar{z}, \tag{18}$$

where α and β take the values X or Y and $H_X = \cos(\bar{x})$ and $H_Y = \sin(\bar{x})$.

The bearing impedances consist of the stiffness and damping coefficients, which are used in a linearized rotor-dynamic model. The critical mass is obtained by finding the whirl frequency canceling the equivalent damping as presented, for example, by Guenat and Schiffmann [21]. The procedure is not repeated here. The non-dimensional critical mass is finally defined as:

$$\bar{m}_{cr} = \frac{m_{cr}\Omega^2 c_0}{R^2 p_{ref}}. \tag{19}$$

3. RESULTS

3.1 Effect of Fluid Molecular Complexity

The effects of the fluid molecular complexity on bearing performance are investigated. Table 1 summarizes the compounds considered in the current analysis along with the relevant properties.

The bearing performance of a rigid journal bearing is numerically investigated for the various compounds. For the purpose of the analysis, a laminar flow regime is assumed by setting the turbulence correction factors to a value of one. The non-dimensional load capacity and critical mass are plotted as a function of the compressibility number Λ in Figure 3. The bearing eccentricity ratio is fixed at $\epsilon = 0.4$. Results are obtained using the Peng-Robinson cubic equation of state for a reduced

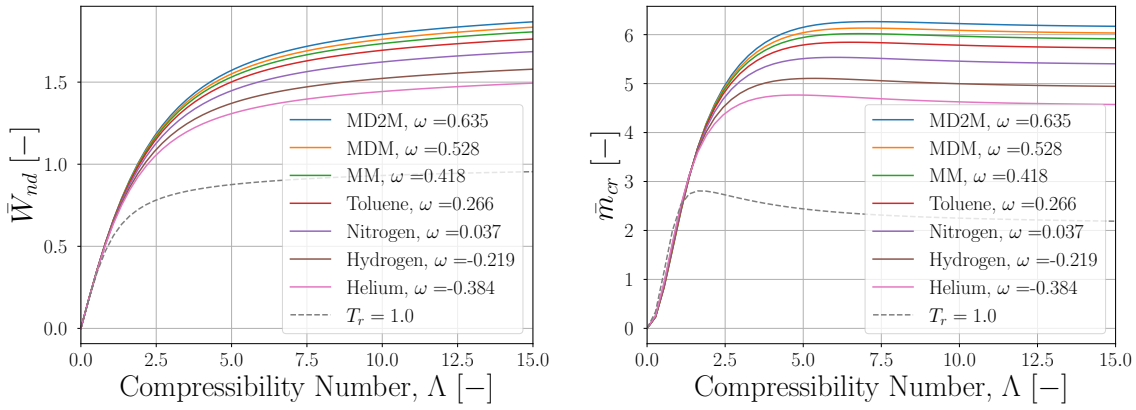

(a) $\bar{W}$. **(b) $\bar{m}_{cr}$.**

FIGURE 3: NON-DIMENSIONAL LOAD CAPACITY $\bar{W}$ AND CRITICAL MASS $\bar{m}_{cr}$ AT $T_r = 1.1$ FOR VARIOUS FLUIDS COMPUTED USING THE PENG-ROBINSON CUBIC EQUATION OF STATE. THE DOTTED LINE REPRESENTS RESULTS FOR $T_r = 1.0$.

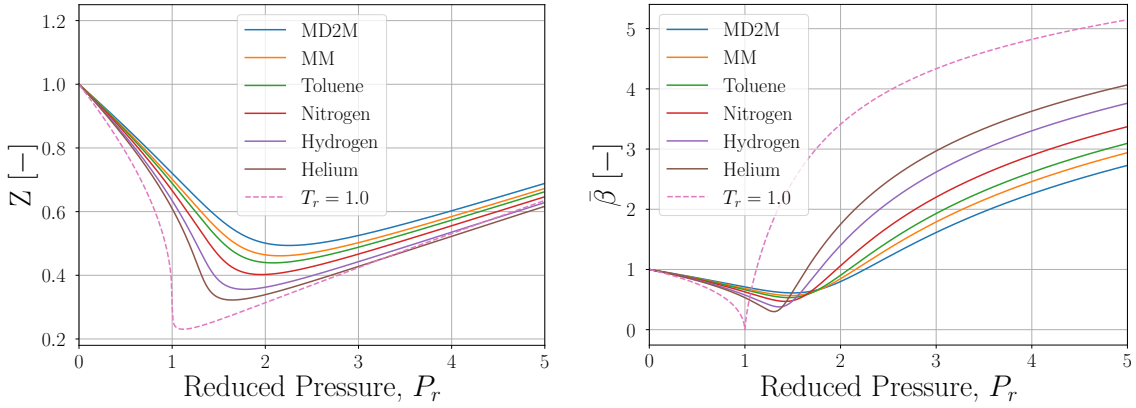

(a) Compressibility factor, Z. **(b) Non-dimensional bulk modulus, $\bar{\beta}$.**

FIGURE 4: COMPRESSIBILITY FACTOR Z AND NON-DIMENSIONAL BULK MODULUS $\bar{\beta}$ AT $T_r = 1.0$ FOR VARIOUS FLUIDS COMPUTED USING THE PENG-ROBINSON CUBIC EQUATION OF STATE. THE DOTTED LINE REPRESENTS RESULTS FOR $T_r = 1.0$.

TABLE 1: FLUID PROPERTIES OF SOME SELECTED FLUIDS.

Fluid	T_c $[K]$	P_c $[bar]$	ρ_c $[kg/m^3]$	ω	Molar Mass $[g/mol]$
Helium	5.2	2.3	69.6	-0.384	4.00
Hydrogen	33.1	13.0	31.3	-0.219	2.02
Nitrogen	126.2	34.0	313.3	0.037	28.01
Toluene	591.8	41.3	292.0	0.266	92.14
MM	518.7	19.3	268.4	0.418	162.38
MDM	565.4	14.4	268.2	0.524	236.53
MD2M	599.4	11.4	268.4	0.635	310.69

pressure of $P_r = 0.8$ and a reduced temperature of $T_r = 1.0$ and $T_r = 1.1$. At the critical temperature ($T_r = 1.0$), both the non-dimensional load capacity and the non-dimensional critical mass are identical for all the considered fluids as indicated by the dotted lines. For a reduced temperature other than the critical temperature (e.g. $T_r = 1.1$), the load capacity and critical mass vary significantly between the different compounds. This difference between working fluids is more significant for increased values of the compressibility number Λ.

The effect of molecular complexity on the bearing performance is explained as follows. The law of corresponding states of Van der Waals indicates that different fluids at the same reduced pressure and temperature exhibit similar volumetric behavior and have approximately the same compressibility factors. The results in Figure 3 are generated using the Peng-Robinson equation of state, although the same conclusions can be drawn using the Soave-Redlich-Kwong (SRK) equation. For the case of the Peng-Robinson (and SRK) cubic equation of state, the deviation of the compressibility factor between working fluids is determined solely by the acentric factor of the fluid [31]. The acentric factor is defined in terms of the reduced vapor pressure at a reduced temperature of $T_r = 0.7$ as:

$$\omega = -1 - \log_{10}\left(P_{vp,r}\right)_{T_r=0.7}. \tag{20}$$

It should be noted that the results shown in Figure 3 are not affected by local variations of the dynamic viscosity in the

thin film. At the considered reduced pressure level, the dynamic viscosity does not vary significantly with pressure at constant temperature. Referring to the compressible Reynolds Equation (1), this leaves the non-dimensional bulk modulus as the main parameter introducing fluid dependence to the density distribution. To understand how molecular complexity affects bearing performance, the relation between the non-dimensional bulk modulus, the compressibility factor Z and the acentric factor ω should thus be considered.

The behavior of the compressibility factor and the non-dimensional bulk modulus is plotted in Figure 4 as a function of the reduced pressure for the considered compounds. Results are again obtained using the Peng-Robinson equation at a reduced temperature of $T_r = 1.0$ and $T_r = 1.1$. A characteristic of the Peng-Robinson (and SRK) equation of state is that the compressibility factor becomes independent of the fluid at the critical temperature as indicated by the dotted line. At temperatures other than the critical temperature, the compressibility factor varies between working fluids as a function of the acentric factor. Moreover, Equation (8) directly relates the non-dimensional bulk modulus to the compressibility factor and the reduced mass density. This indicates that, within the limits of validity of the considered cubic equations of state, the non-dimensional bulk modulus is a function of reduced temperature and pressure and varies between working fluids only as a function of the acentric factor. This observation is in agreement with the plots of $\bar{\beta}$ in Figure 4.

Equations of state like the Van der Waals and Redlich-Kwong model neglect any anisotropic molecular interactions [32]. The acentric factor was used by Soave as an additional parameter supplementing the Redlich-Kwong equation of state to account for the effects of polarity and non-spherical shapes of the molecules [31]. In general, fluids with more complex molecules tend to have larger values of the acentric factor. A measure for the molecular complexity of a fluid [10] is the number of active degrees of freedom N, defined as:

$$N = \frac{2}{\delta_\infty (T_c)} = \frac{2c_{v_\infty}(T_c)}{R}, \tag{21}$$

in which the ideal gas isochoric specific heat is evaluated at the critical temperature. The acentric factor is plotted versus the number of active degrees of freedom in Figure 5 for the considered fluids. Fluids with larger molecular complexity tend to have a higher acentric factor at least for fluids belonging to the same class (e.g. hydro-fluorocarbons, hydrocarbons, siloxanes).

The current discussion suggests that both the non-dimensional load capacity and critical mass are affected by the acentric factor and thus the molecular complexity of the fluid. In the limit of an ideal gas, however, the non-dimensional bulk modulus reduces to a constant value of $\bar{\beta}_{ref} = 1$ as shown by Equation (9). Therefore, the molecular complexity of the fluid only affects the bearing performance of dense vapors or supercritical fluids where non-ideal thermodynamic effects are significant. Furthermore, the increased molecular complexity of a fluid seems to reduce the impact of non-ideal thermodynamic effects on bearing performance.

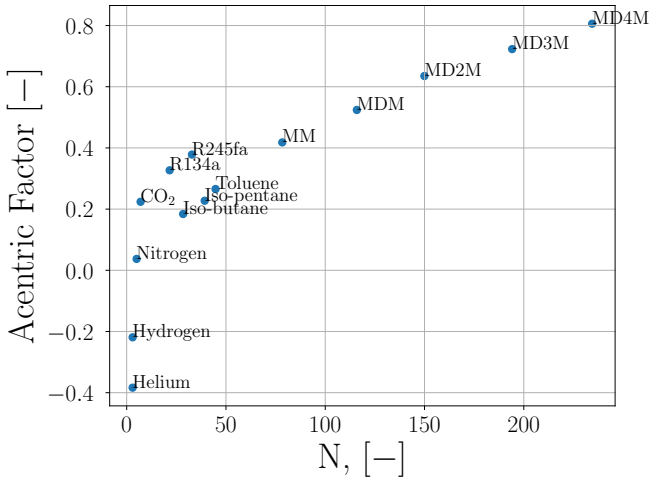

FIGURE 5: ACENTRIC FACTOR AS A MEASURE OF MOLECULAR COMPLEXITY PLOTTED VERSUS THE NUMBER OF ACTIVE DEGREES OF FREEDOM (*N*).

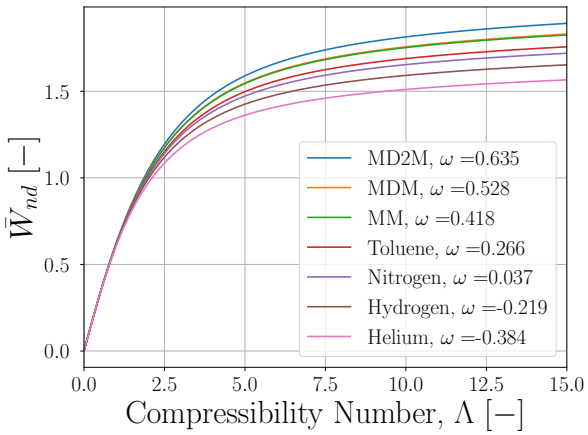

FIGURE 6: NON-DIMENSIONAL LOAD CAPACITY $\bar{W}$ AT $T_r = 1.1$ FOR VARIOUS FLUIDS COMPUTED USING MULTI-PARAMETER EQUATIONS OF STATE [19].

To confirm the observations obtained using the Peng-Robinson equation, the analysis is repeated utilizing the more complex Helmholtz-based multi-parameter equations of state models available in [19]. The resulting non-dimensional load capacity is shown in Figure 6. In general, the results confirm the dependence of the bearing performance on the acentric factor for increased bearing speed numbers. For siloxane MM and MDM, however, similar values are obtained for the non-dimensional load capacity even though both compounds have different values of ω. The differences in bearing performance between different lubricant fluids are therefore not solely related to the acentric factor. However, the results obtained using the multi-parameter equations of state seem to confirm the discussed qualitative observations. Similar conclusions can be drawn by plotting the non-dimensional critical mass, which has been omitted for brevity.

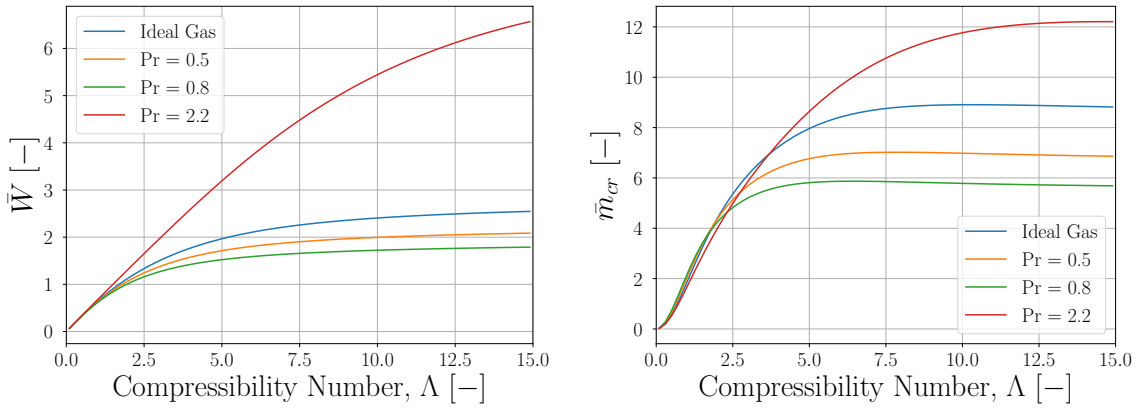

(a) $\bar{W}$. (b) $\bar{m}_{cr}$.

FIGURE 7: NON-DIMENSIONAL LOAD CAPACITY $\bar{W}$ AND CRITICAL MASS $\bar{m}_{cr}$ AS A FUNCTION OF COMPRESSIBILITY NUMBER AT $\epsilon = 0.4$ FOR SILOXANE MM AT VARIOUS THERMODYNAMIC CONDITIONS.

3.2 Effect of Non-Ideal Thermodynamic Properties

The numerical model is used to study the influence of non-ideal thermodynamic effects on the performance of rigid journal bearings operating with siloxane MM in different thermodynamic states. The considered thermodynamic conditions along with the corresponding non-dimensional parameters characterizing the non-ideal thermodynamic effects are reported in Table 2. The operating points are also shown on the reduced *T-s* thermodynamic plane for siloxane MM in Figure 2 along with contours of the non-dimensional bulk modulus $\bar{\beta}$. The operating points are chosen sufficiently far from the thermodynamic critical point such that the compressible Reynolds Equation (1) remains valid [23]. The values of the non-dimensional load capacity and critical mass obtained at the given thermodynamic conditions are compared to those for MM in ideal gas conditions.

Parameter	Point 1	Point 2	Point 3
T_r	1.1	1.1	1.1
P_r	0.5	0.8	2.2
Z	0.864	0.775	0.423
$\bar{\beta}$	0.857	0.760	1.068
γ	1.050	1.082	1.358
γ_{Pv}	0.900	0.822	1.451

TABLE 2: THERMODYNAMIC REFERENCE STATES CONSIDERED FOR ANALYZING THE INFLUENCE OF NON-IDEAL THERMODYNAMIC EFFECTS ON BEARING PERFORMANCE.

Figure 7a shows the variation of the non-dimensional load capacity with Λ, for the four considered thermodynamic states. At low compressibility numbers, the influence of the thermodynamic state is negligible. As the compressibility number increases, the bearings operating with the working fluid at $P_r = 0.8$ and $P_r = 0.5$ show a lower load capacity compared to the operation with MM in an ideal gas state. This observation is in agreement with the conclusions drawn by Guenat and Schiffmann [21]. Conversely, the non-dimensional load capacity significantly increases at the supercritical pressure $P_r = 2.2$.

The influence of the different thermodynamic states is explained using Figure 8. The figure displays the circumferential distribution of the non-dimensional density and pressure at mid-span of the bearing for the different operating conditions. An eccentricity ratio of $\epsilon = 0.6$ and a compressibility number of $\Lambda = 3.0$ are used to generate the plots. From observation of the compressible Reynolds Equation (1) it is apparent that a reduced non-dimensional bulk modulus decreases the significance of the diffusive terms on the left-hand side of the equation. This is reflected in Figure 8a, which shows a stronger increase in the non-dimensional density for $\bar{\beta} < 1$ as compared to thermodynamic states in which $\bar{\beta} \geq 1$. The corresponding non-dimensional pressure distribution is shown in Figure 8b. In contrast to the density, a stronger increase in the pressure is observed for increasing values of the non-dimensional bulk modulus. This in turn leads to increased values of the non-dimensional load capacity. For increased values of $\bar{\beta}$, a relatively small increase in density can cause a strong increase in pressure. The bulk modulus can therefore also be interpreted as a measure of the stiffness of the fluid at a particular thermodynamic state. For example, liquids tend to have a relatively large stiffness compared to fluids in non-ideal states near the critical point or saturated vapor line.

The non-dimensional critical mass is plotted as a function of the compressibility number in Figure 7b for the different thermodynamic conditions. Similar trends are observed as compared to those obtained for the non-dimensional load capacity. Significant deviations only occur at high values of the compressibility number. In particular, the critical mass is reduced when the working fluid is in non-ideal states for which $\gamma_{Pv} < \gamma$ or for which $\bar{\beta} < 1$. The results are in agreement with those presented by Guenat and Schiffmann [21].

3.3 GFB Stiffness & Damping Coefficients

The influence of working fluid and non-ideal thermodynamic effects on gas foil bearing stiffness and damping coefficients is finally considered. Non-dimensional stiffness and damping coefficients are plotted as a function of the non-dimensional excitation frequency in Figure 9. Results are obtained for a gas foil bearing

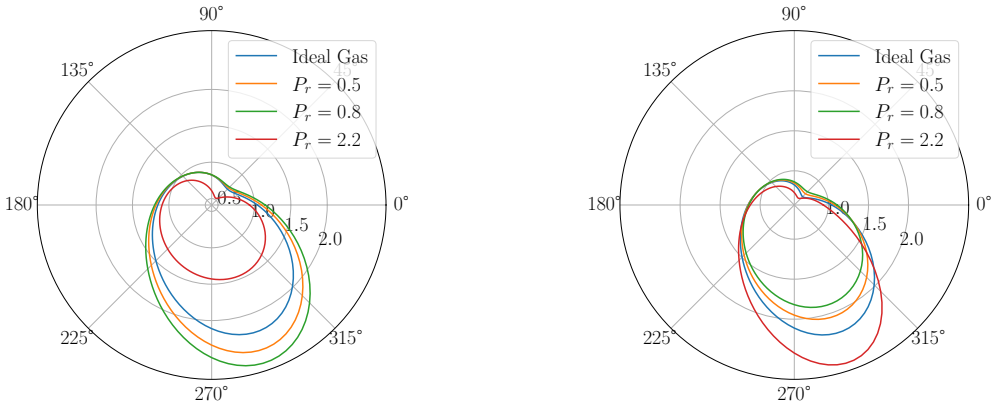

(a) Non-dimensional density **(b) Non-dimensional pressure**

FIGURE 8: POLAR PLOTS OF THE NON-DIMENSIONAL DENSITY AND PRESSURE AROUND THE CIRCUMFERENCE OF THE BEARING AT MID-SPAN. GREY CIRCLES INDICATE ISO-DENSITY OR ISO-PRESSURE LINES.

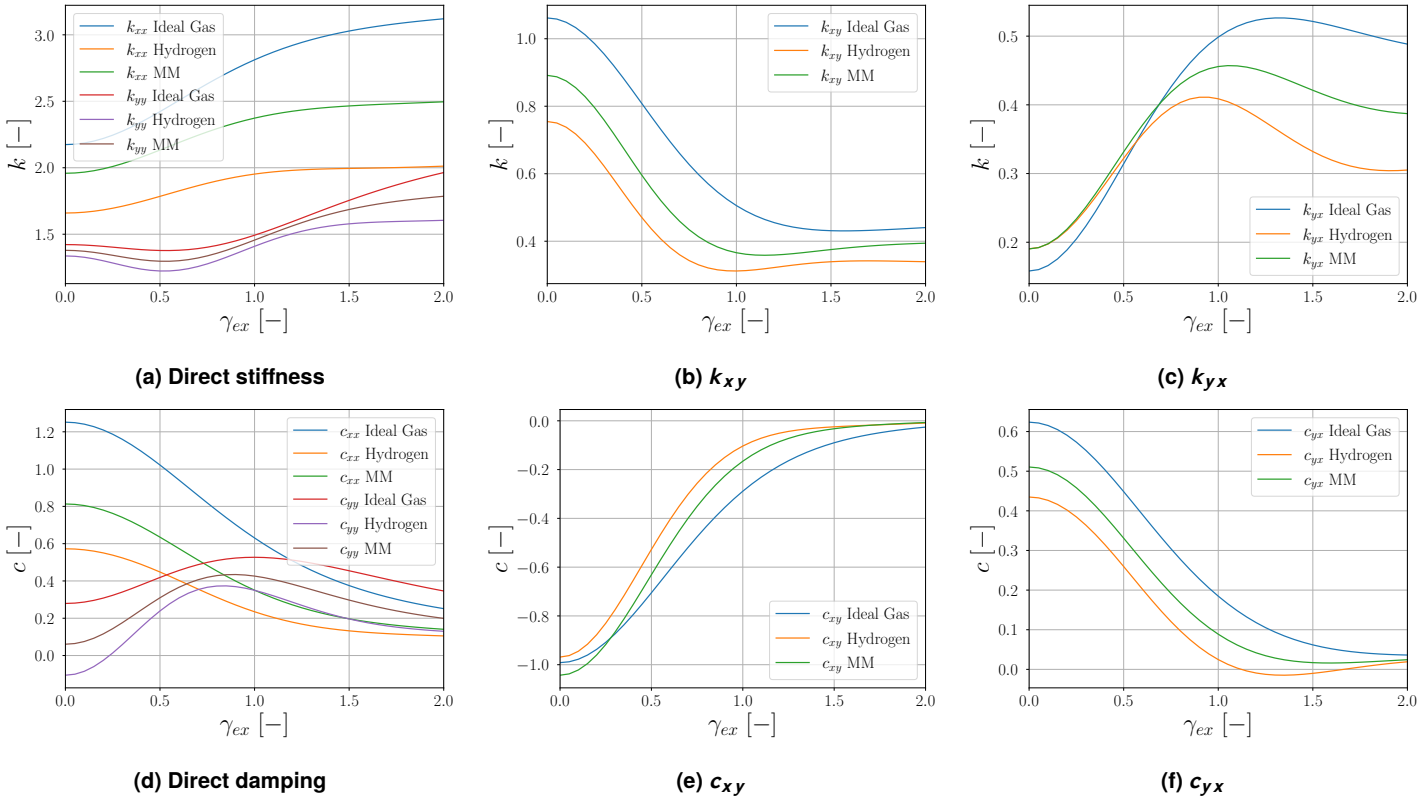

(a) Direct stiffness **(b) k_{xy}** **(c) k_{yx}**

(d) Direct damping **(e) c_{xy}** **(f) c_{yx}**

FIGURE 9: NON-DIMENSIONAL STIFFNESS AND DAMPING COEFFICIENTS.

with an axial width-to-diameter ratio of $L/D = 1$ and a bump foil structural compliance ratio of $S = 0.5$. The bearing operates at a compressibility number of $\Lambda = 1.0$ and an equilibrium eccentricity of $\epsilon = 0.8$. Finally, the structural loss factor is set to $\gamma_S = 0$.

Lubrication using hydrogen and siloxane MM is considered as these fluids have significantly different values for the acentric factor. The reference thermodynamic state of both fluids corresponds to a reduced pressure and temperature of $P_r = 0.94$ and $T_r = 1.1$ for which $\bar{\beta} < 1$. Results are compared to a bearing in which the lubricant behaves as an ideal gas. Figure 9 shows an increase in the direct stiffness components (k_{xx} and k_{yy}) with excitation frequency. The cross-coupled stiffness component k_{xy} tends to decrease with excitation frequency. The k_{yx} component increases until the synchronous frequency ($\gamma_{ex} = 1$) and decreases at higher frequencies. Both the direct and cross-coupled damping coefficients shown in Figure 9 tend to decrease at high excitation frequencies. These observations are in agreement with results presented by Kim and San Andrés [29].

Comparing the different bearing operating conditions, the

figures show that both the direct and cross-coupled stiffness and damping coefficients decrease in magnitude due to the non-ideal thermodynamic effects. This corroborates the interpretation of the bulk modulus as a measure of fluid stiffness. Furthermore, referring to Figure 7b, the net result is a decreased bearing stability as indicated by the reduced critical mass. The effect is more pronounced for hydrogen as compared to MM. This shows the reduced influence of non-ideal thermodynamic effects for working fluids made by more complex molecules in correspondence with the discussion in the previous section.

4. CONCLUSION

The influence of non-ideal thermodynamic effects and molecular complexity of the working fluid on the performance of gas bearings has been investigated. In particular, the non-dimensional load capacity and critical mass of rigid journal bearings and the stiffness and damping coefficients of gas foil bearings have been considered. The analysis was performed using equations of state of varying complexity. The following conclusions can be drawn from this work.

1. The influence of non-ideal thermodynamic effects on gas bearing performance can be understood by analysis of the non-dimensional bulk modulus. The non-dimensional bulk modulus is directly related to the reduced density and the compressibility factor. Reduced values of the non-dimensional bulk modulus near the thermodynamic critical point or saturated vapor line decrease bearing performance.

2. The main parameter characterizing the influence of molecular complexity on gas bearing performance is shown to be the acentric factor. For complex fluids with large acentric factors, the impact of non-ideal thermodynamic effects on non-dimensional bearing load capacity and rotor-dynamic characteristics is less pronounced.

APPENDIX A. PERTURBED REYNOLDS EQUATION

The perturbed quantities as presented in section 2 are substituted into the unsteady Reynolds Equation (1). Zeroth and first-order terms in the density can be grouped and separated to obtain a set of second-order differential equations. The zeroth order terms govern the steady-state density field as:

$$\frac{\partial}{\partial\bar{x}}\left(\bar{h}_0^3 G_{0x}\bar{\kappa}_{Te0}\frac{\partial\bar{\rho}_0}{\partial\bar{x}}\right)+\frac{\partial}{\partial\bar{z}}\left(\bar{h}_0^3 G_{z0}\bar{\kappa}_{Te0}\frac{\partial\bar{\rho}_0}{\partial\bar{z}}\right)=\Lambda\frac{\partial\left(\bar{\rho}_0\bar{h}_0\right)}{\partial\bar{x}} \tag{22}$$

The perturbed Reynolds equation for ρ_{1X} and ρ_{1Y} accounting for the effect of bump foil deflections is written as:

$$\begin{aligned}
&\frac{\partial}{\partial\bar{x}}\left(\bar{h}_0^3\bar{\kappa}_{Te0}G_{x0}\frac{\partial\bar{\rho}_{1\alpha}}{\partial\bar{x}}\right)+\frac{\partial}{\partial\bar{z}}\left(\bar{h}_0^3\bar{\kappa}_{Te0}G_{z0}\frac{\partial\bar{\rho}_{1\alpha}}{\partial\bar{z}}\right)+\\
&\frac{\partial}{\partial\bar{x}}\left(\bar{h}_0^3\left(\frac{\partial\bar{\kappa}_{Te}}{\partial\bar{\rho}}\right)_0\bar{\rho}_{1\alpha}G_{x0}\frac{\partial\bar{\rho}_0}{\partial\bar{x}}\right)+\frac{\partial}{\partial\bar{z}}\left(\bar{h}_0^3\left(\frac{\partial\bar{\kappa}_{Te}}{\partial\bar{\rho}}\right)_0\bar{\rho}_{1\alpha}G_{z0}\frac{\partial\bar{\rho}_0}{\partial\bar{z}}\right)+\\
&\frac{\partial}{\partial\bar{x}}\left(\bar{h}_0^3\bar{\kappa}_{Te0}\left[\left(\frac{\partial G_x}{\partial\bar{\rho}}\right)_0+\left(\frac{\partial G_x}{\partial\bar{\mu}}\right)_0\left(\frac{\partial\bar{\mu}}{\partial\bar{\rho}}\right)_0\right]\bar{\rho}_{1\alpha}\frac{\partial\bar{\rho}_0}{\partial\bar{x}}\right)+\\
&\frac{\partial}{\partial\bar{z}}\left(\bar{h}_0^3\bar{\kappa}_{Te0}\left[\left(\frac{\partial G_z}{\partial\bar{\rho}}\right)_0+\left(\frac{\partial G_z}{\partial\bar{\mu}}\right)_0\left(\frac{\partial\bar{\mu}}{\partial\bar{\rho}}\right)_0\right]\bar{\rho}_{1\alpha}\frac{\partial\bar{\rho}_0}{\partial\bar{z}}\right)+\\
&\frac{\partial}{\partial\bar{x}}\left(3\bar{h}_0^2\frac{S}{(1+i\gamma_S)}\delta\bar{p}_{1\alpha}\bar{\kappa}_{Te0}G_{x0}\frac{\partial\bar{\rho}_0}{\partial\bar{x}}\right)+\\
&\frac{\partial}{\partial\bar{z}}\left(3\bar{h}_0^2\frac{S}{(1+i\gamma_S)}\delta\bar{p}_{1\alpha}\bar{\kappa}_{Te0}G_{z0}\frac{\partial\bar{\rho}_0}{\partial\bar{z}}\right)=\\
&-\frac{\partial}{\partial\bar{x}}\left(\bar{h}_0^2\bar{\kappa}_{Te0}\left[3G_{x0}+\left(\frac{\partial G_x}{\partial\bar{h}}\right)_0\right]H_\alpha\frac{\partial\bar{\rho}_0}{\partial\bar{x}}\right)-\\
&\frac{\partial}{\partial\bar{z}}\left(\bar{h}_0^2\bar{\kappa}_{Te0}\left[3G_{z0}+\left(\frac{\partial G_z}{\partial\bar{h}}\right)_0\right]H_\alpha\frac{\partial\bar{\rho}_0}{\partial\bar{z}}\right)+\\
&\Lambda\frac{\partial}{\partial\bar{x}}\left(\bar{\rho}_0H_\alpha+\bar{\rho}_0\frac{S}{(1+i\gamma_S)}\delta\bar{p}_{1\alpha}+\bar{\rho}_{1\alpha}\bar{h}_0\right)+\\
&i2\gamma\Lambda\left(\bar{\rho}_0H_\alpha+\bar{\rho}_0\frac{S}{(1+i\gamma_S)}\delta\bar{p}_{1\alpha}+\bar{\rho}_{1\alpha}\bar{h}_0\right)
\end{aligned} \tag{23}$$

Where $\alpha = X$ and $H_X = \cos(\bar{x})$ for $\bar{\rho}_{1X}$ and $\alpha = Y$ and $H_Y = \sin(\bar{x})$ for $\bar{\rho}_{1Y}$. Finally, $\delta\bar{p}_{1\alpha}$ represents the axially averaged perturbation in the pressure in response to a journal displacement.

REFERENCES

[1] Colonna, P., Casati, E., Trapp, C., Mathijssen, T., Larjola, J., Turunen-Saaresti, T. and Uusitalo, A. "Organic Rankine Cycle Power Systems: From the Concept to Current Technology, Applications, and an Outlook to the Future." *Journal of Engineering for Gas Turbines and Power* Vol. 137 No. 10 (2015): 100801. DOI 10.1115/1.4029884.

[2] Casey, M., Krähenbühl, D. and Zwyssig, C. "The design of ultra-high-speed miniature centrifugal compressors." *10th European Conference on Turbomachinery Fluid Dynamics and Thermodynamics, ETC 2013* (2014): pp. 506–519.

[3] Lee, Y., Park, D., Kim, T.H. and Sim, K. "Development and Performance Measurement of Oil-Free Turbocharger Supported on Gas Foil Bearings." *Journal of Engineering for Gas Turbines and Power* Vol. 134 No. 3 (2012): 032506. DOI 10.1115/1.4004719.

[4] Zagarola, M.V. and McCormick, J.A. "High-capacity turbo-Brayton cryocoolers for space applications." *Cryogenics* Vol. 46 No. 2 (2006): pp. 169–175. DOI 10.1016/j.cryogenics.2005.11.018.

[5] Kadyk, T., Schenkendorf, R., Hawner, S., Yildiz, B. and Römer, U. "Design of Fuel Cell Systems for Aviation: Representative Mission Profiles and Sensitivity Analyses." *Frontiers in Energy Research* Vol. 7 (2019): p. 35. DOI 10.3389/fenrg.2019.00035.

[6] Schiffmann, J. and Favrat, D. "Experimental investigation of a direct driven radial compressor for domestic heat pumps."

International Journal of Refrigeration Vol. 32 No. 8 (2009): pp. 1918–1928. DOI 10.1016/j.ijrefrig.2009.07.006.

[7] Giuffré, A., Colonna, P. and Pini, M. "The Effect of Size and Working Fluid on the Multi-Objective Design of High-Speed Centrifugal Compressors." *International Journal of Refrigeration* Vol. 143 (2022): pp. 43–56. DOI 10.1016/j.ijrefrig.2022.06.023.

[8] Conboy, T., Wright, S., Pasch, J., Fleming, D., Rochau, G. and Fuller, R. "Performance Characteristics of an Operating Supercritical CO_2 Brayton Cycle." *Journal of Engineering for Gas Turbines and Power* Vol. 134 No. 11 (2012): 111703. DOI 10.1115/1.4007199.

[9] DellaCorte, C., Radil, K., Bruckner, R. and Howard, S. "Design, Fabrication, and Performance of Open Source Generation I and II Compliant Hydrodynamic Gas Foil Bearings." *Tribology Transactions* Vol. 51 (2008): pp. 254–264. DOI 10.1080/10402000701772579.

[10] Guardone, A., Colonna, P., Pini, M. and Spinelli, A. "Non-ideal Compressible Fluid Dynamics of Dense Vapors and Supercritical Fluids." *Annual Review of Fluid Mechanics* Vol. 56 (2024): pp. 241–269. DOI 10.1146/annurev-fluid-120720-033342.

[11] Giuffré, A., Colonna, P. and Pini, M. "Design Optimization of a High-Speed Twin-Stage Compressor for Next-Gen Aircraft Environmental Control System." *Journal of Engineering for Gas Turbines and Power* Vol. 145 No. 3 (2023): 031017. DOI 10.1115/1.4056022.

[12] Giuffré, A. and Pini, M. "Design Guidelines for Axial Turbines Operating With Non-Ideal Compressible Flows." *Journal of Engineering for Gas Turbines and Power* Vol. 143 No. 1 (2021): 011004. DOI 10.1115/1.4049137.

[13] Tosto, F., Lettieri, C., Pini, M. and Colonna, P. "Dense-Vapor Effects in Compressible Internal Flows." *Physics of Fluids* Vol. 33 No. 8 (2021): 086110. DOI 10.1063/5.0058075.

[14] DellaCorte, C. and Valco, M. "Load Capacity Estimation of Foil Air Journal Bearings for Oil-Free Turbomachinery Applications." *Tribology Transactions* Vol. 43 No. 4 (2000): pp. 795–801. DOI 10.1080/10402000008982410.

[15] DellaCorte, C. "Stiffness and Damping Coefficient Estimation of Compliant Surface Gas Bearings for Oil-Free Turbomachinery." *Tribology Transactions* Vol. 54 No. 4 (2011): pp. 674–684. DOI 10.1080/10402004.2011.589966.

[16] Heshmat, H., Walowit, J. A. and Pinkus, O. "Analysis of Gas-Lubricated Foil Journal Bearings." *Journal of Tribology* Vol. 105 No. 4 (1983): pp. 647–655. DOI 10.1115/1.3254697.

[17] Bruckner, R. "Windage Power Loss in Gas Foil Bearings and the Rotor-Stator Clearance of High Speed Generators Operating in High Pressure Environments." *Proceedings of the ASME Turbo Expo 2009: Power for Land, Sea, and Air*, Vol. 5: Microturbines and Small Turbomachinery; Oil and Gas Applications: pp. 263–270. Orlando, Florida, USA, June 8-12, 2009. DOI 10.1115/GT2009-60118.

[18] Conboy, T. M. "Real-Gas Effects in Foil Thrust Bearings Operating in the Turbulent Regime." *Journal of Tribology* Vol. 135 No. 3 (2013): 031703. DOI 10.1115/1.4024048.

[19] Lemmon, E. W., Bell, I. H., Huber, M. L. and McLinden, M. O. "NIST Standard Reference Database 23: Reference Fluid Thermodynamic and Transport Properties-REFPROP, Version 10.0, National Institute of Standards and Technology." (2018). DOI 10.18434/T4/1502528.

[20] Kim, D. "Design Space of Foil Bearings for Closed-Loop Supercritical CO_2 Power Cycles Based on Three-Dimensional Thermohydrodynamic Analyses." *Journal of Engineering for Gas Turbines and Power* Vol. 138 No. 3 (2016): 032504. DOI 10.1115/1.4031433.

[21] Guenat, E. and Schiffmann, J. "Real-Gas Effects on Aerodynamic Bearings." *Tribology International* Vol. 120 (2018): pp. 358–368. DOI 10.1016/j.triboint.2018.01.008.

[22] Reynolds, O. "IV. On the theory of lubrication and its application to Mr. Beauchamp tower's experiments, including an experimental determination of the viscosity of olive oil." *Philosophical Transactions of the Royal Society A* Vol. 177 (1886): pp. 157–234. DOI 10.1098/rstl.1886.0005.

[23] Chien, S. Y., Cramer, M. S. and Untaroiu, A. "Compressible Reynolds Equation for High-Pressure Gases." *Physics of Fluids* Vol. 29 No. 11 (2017): 116101. DOI 10.1063/1.5000827.

[24] Constantinescu, V. N. "On Turbulent Lubrication." *Proceedings of the Institution of Mechanical Engineers* Vol. 173 No. 1 (1959): pp. 881–900. DOI 10.1243/PIME_PROC_1959_173_068_02.

[25] Ng, C. and Pan, C. H. T. "A Linearized Turbulent Lubrication Theory." *Journal of Basic Engineering* Vol. 87 No. 3 (1965): pp. 675–682. DOI 10.1115/1.3650640.

[26] Hirs, G. G. "A Bulk-Flow Theory for Turbulence in Lubricant Films." *Journal of Lubrication Technology* Vol. 95 No. 2 (1973): pp. 137–145. DOI 10.1115/1.3451752.

[27] Giuffré, A. and Pini, M. "NiceProp: An Interactive Python-Based Educational Tool for Non-Ideal Compressible Fluid Dynamics." *SoftwareX* Vol. 17 (2022): 100897. DOI 10.1016/j.softx.2021.100897.

[28] Bell, I. H., Wronski, J., Quoilin, S. and Lemort, V. "Pure and Pseudo-Pure Fluid Thermophysical Property Evaluation and the Open-Source Thermophysical Property Library CoolProp." *Industrial & Engineering Chemistry Research* Vol. 53 No. 6 (2014): pp. 2498–2508. DOI 10.1021/ie4033999.

[29] San Andrés, L. and Kim, T.H. "Heavily Loaded Gas Foil Bearings: A Model Anchored to Test Data." *Journal of Engineering for Gas Turbines and Power* Vol. 130 No. 1 (2008): 012504. DOI 10.1115/1.2770494.

[30] San Andrés, L. and Kim, T.H. "Analysis of Gas Foil Bearings Integrating FE Top Foil Models." *Tribology International* Vol. 42 No. 1 (2009): pp. 111–120. DOI 10.1016/j.triboint.2008.05.003.

[31] Invernizzi, C.M. *Closed Power Cycles: Thermodynamic Fundamentals and Applications*. Lecture Notes in Energy, Springer London (2013).

[32] Guardone, A. and Argrow, B. M. "Nonclassical Gasdynamic Region of Selected Fluorocarbons." *Physics of Fluids* Vol. 17 No. 11 (2005): 116102. DOI 10.1063/1.2131922.